

Influence of Interim Alkyl Chain Length on Phase Transitions and Wide-Band Reflective Behaviors of Side-Chain Liquid Crystalline Elastomers with Binaphthalene Crosslinkings

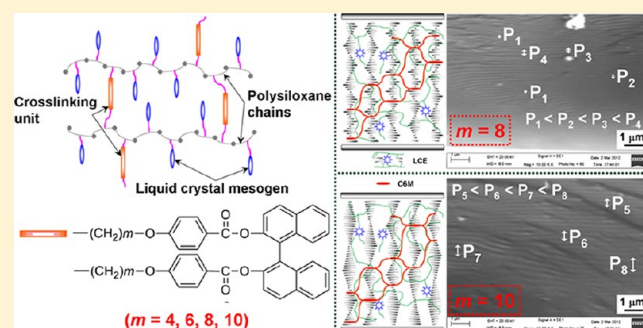
Xiaojuan Wu,[†] Hui Cao,[†] Renwei Guo,[†] Kexuan Li,[†] Feifei Wang,[†] Yanzi Gao,[†] Wenhuan Yao,[†] Lanying Zhang,[‡] Xiaofang Chen,[§] and Huai Yang^{*,†,‡,§}

[†]Department of Materials Physics and Chemistry, School of Materials Science and Engineering, University of Science and Technology Beijing, Beijing 100083, P. R. China

[‡]Department of Materials Science and Engineering, College of Engineering, Peking University, Beijing 100871, P. R. China

[§]Department of Polymer Science and Engineering and The Key Laboratory of Polymer Chemistry and Physics of Ministry of Education, College of Chemistry, Peking University, Beijing 100871, P. R. China

ABSTRACT: A series of side-chain polysiloxane liquid crystalline elastomers, E-C m (where m is the number of carbon atoms in the interim alkyl groups, and $m = 4, 6, 8, 10$), with binaphthalene derivatives as crosslinkings, were designed and synthesized. The mesophase structures of these elastomers were dependent on the value of m . The elastomers with $m \leq 8$ could form cholesteric (Ch) phases, while both smectic A and Ch phases could be formed for the elastomer with $m = 10$. Blue phases can be achieved when $m \geq 8$. Besides, the helical twisting power (HTP) of all the elastomers exhibits a turning point with changing temperature. Both the turning temperature and HTP have an apparent dependence on the value of m . By adjusting the interim alkyl chain length in the elastomers, both visible and near-infrared light wide-band reflective films can be obtained. The broadband reflection mechanism was confirmed by SEM investigations.



INTRODUCTION

Liquid crystalline elastomers (LCEs) represent fascinating materials of soft matter, combining the properties of polymeric elastomers (entropy elasticity) with liquid crystals (self-organization). To achieve liquid crystallinity, flexible spacers are usually introduced in LCEs to decouple the dynamics of the main chain and the mesogenic side groups.¹ If the side groups (at least partially) are chiral, a helically twisted structure (the so-called cholesteric structure) can be obtained. Recently, LCEs have received a lot of interest,^{2–5} owing to their special optical,^{6,7} thermal,^{8,9} mechanical,^{10–13} and electrical^{14–16} properties. Correspondingly, they exhibit potential applications in actuators,^{17–20} shape-memory materials,^{21–25} and photonics.^{26–28} LCEs have also been actively investigated as an alternative for piezoelectrics, hydrogels, conducting polymers, dielectric elastomers, and many other polymer systems for use as artificial muscles or actuators.^{29,30}

Cholesteric liquid crystalline elastomers (ChLCEs) and polymers hold inherent characteristics of cholesteric liquid crystal (CLC) and present promising applications in wide-band reflective devices.^{31–34} Because of the unique helical supramolecular structure, CLC can selectively reflect circularly polarized incident light with the same handedness as its helical axis.³⁵ At normal incidence, the mean reflection wavelength, $\lambda = nP$, where $n = (n_o + n_e)/2$ is the average of the ordinary (n_o)

and extraordinary (n_e) refractive indices of the CLC, P is the cholesteric pitch corresponding to the length of a 2π molecular rotation. The reflected bandwidth ($\Delta\lambda$) is given by $\Delta\lambda = (n_e - n_o)P = \Delta nP$, where $\Delta n = n_e - n_o$ is the birefringence of the liquid crystal. Because a Δn value for colorless organic material is generally smaller than 0.3, the bandwidth of a single-pitch CLC in visible region is less than 100 nm, which is insufficient for some applications such as brightness enhancement films, wide-band reflective polarizers, and so on. To broaden the bandwidth, forming a pitch gradient^{36,37} or a nonuniform pitch distribution^{38,39} in a stable CLC film is usually used.

Chiral binaphthyl derivatives are widely used as high HTP chiral dopants in host liquid crystals to form CLCs.^{40–43} Studies on LCEs derived from chiral binaphthyl derivatives are less reported. Herein, we report the synthesis and characterization of a series of side-chain LCEs, E-C m (where m is the number of carbon atoms in the interim alkyl groups, and $m = 4, 6, 8, 10$), with binaphthyl derivatives as crosslinkings and cholesterol derivatives as mesogenic groups. We examined the liquid crystallinity and HTP of these elastomers using various techniques, such as POM, DSC, WAXD, and Cano-wedge, and

Received: March 27, 2012

Revised: May 8, 2012

Published: June 29, 2012

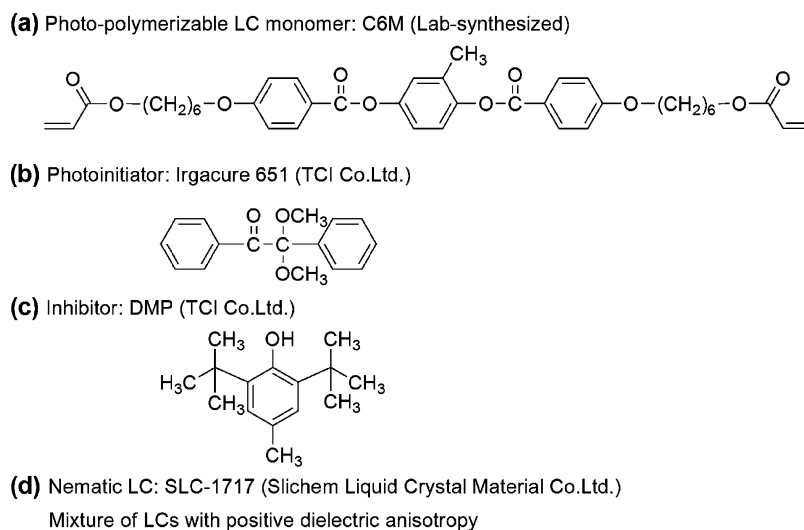


Figure 1. Chemical structures of the materials used.

found that both the liquid crystal (LC) phase structures and helical twisting behaviors were affected by the interim alkyl chain length. Furthermore, visible and near-infrared light wide-band reflective films with nonuniform pitch distributions were obtained by using elastomers with short and long interim alkyl chain length, respectively. The microstructures of the films were investigated by SEM observations.

EXPERIMENTAL SECTION

Materials. Polymethylhydrosiloxane (PMHS, $M_n = 390$, Sigma-Aldrich) and H_2PtCl_6 (Sinopharm Chemical Reagent Co. Ltd.) were used as received. Toluene was distilled from Na/benzophenone under N_2 for at least 8 h until the solution turned blue. 1,1'-Binaphthyl-2,2'-diol, ethyl 4-hydroxy benzoate, 4-bromobut-1-ene, 6-bromohex-1-ene, 8-bromooct-1-ene, 10-bromodec-1-ene, cholesterol, and other reagents and solvents were used as received from commercial sources. Besides, a room temperature nematic LC, SLC-1717 ($n_o = 1.519$, $n_e = 1.720$, Slichem Liquid Crystal Material Co. Ltd.), a photopolymerizable LC monomer, 1,4-di-[4-(6-acryloyloxy) hexyloxy benzoyloxy]-2-methyl benzene (C6M), a photoinitiator, 2,2-dimethoxy-1,2-diphenylethaneone (IRG651, TCI Co. Ltd.), and an inhibitor, 2,6-di-tert-butyl-4-methylphenol (DMP, TCI Co. Ltd.) were used. C6M was synthesized according to the method suggested by Broer.⁴⁴ Figure 1 shows the chemical structures of these materials.

Characterization and Measurements. 1H NMR (300 MHz) spectra were recorded on a Bruker DMX-300 spectrometer using deuterated chloroform ($CDCl_3$) with tetramethylsilane as the internal standard at room temperature.

Fourier transform infrared spectroscopy (FT-IR) was conducted on a Perkin-Elmer Spectrum One in solid state by the KBr method with wavenumber ranging from 400 to 4000 cm^{-1} .

Thermogravimetric analysis (TGA) was performed on a STA 449 F3 instrument at a heating rate of $10\text{ }^\circ\text{C}/\text{min}$ in a nitrogen atmosphere.

Differential scanning calorimetry (DSC) examination was carried out on a Perkin-Elmer Pyris 6 calorimeter with a heating and a cooling rate of $10\text{ }^\circ\text{C}/\text{min}$ under a dry nitrogen purge.

Polarized optical microscopy (POM) was carried out to observe the LC textures of the samples on a Olympus BX51 microscope with a Linkam THMS-600 hot stage calibrated to an accuracy of $\pm 0.1\text{ }^\circ\text{C}$.

One-dimensional (1D) wide-angle X-ray diffraction (WAXD) experiments were carried out on a Philips X'Pert Pro diffractometer with a 3 KW ceramic tube as the X-ray source ($Cu\ K\alpha$) and an X'celerator detector.

Scanning electron microscopy (SEM) was used to observe the morphology of the fractured surface of the wide-band reflective films on a Zeiss EVO18 instrument.

Synthesis of Monomers. The synthetic routes of the cross-linkings, 1,1'-binaphthyl-2,2'-diyl bis(4-(alkenyl-oxy)benzoate (L-Cm), and the liquid crystalline monomers, cholesteryl-4-alkenyl-oxybenzoate (M-Cm, where m is the number of carbon atoms in the alkenyl groups, and $m = 4, 6, 8, 10$), are shown in Scheme 1. The experimental details of monomer synthesis and characterization are described below using L-C10 and M-C10 as an example.

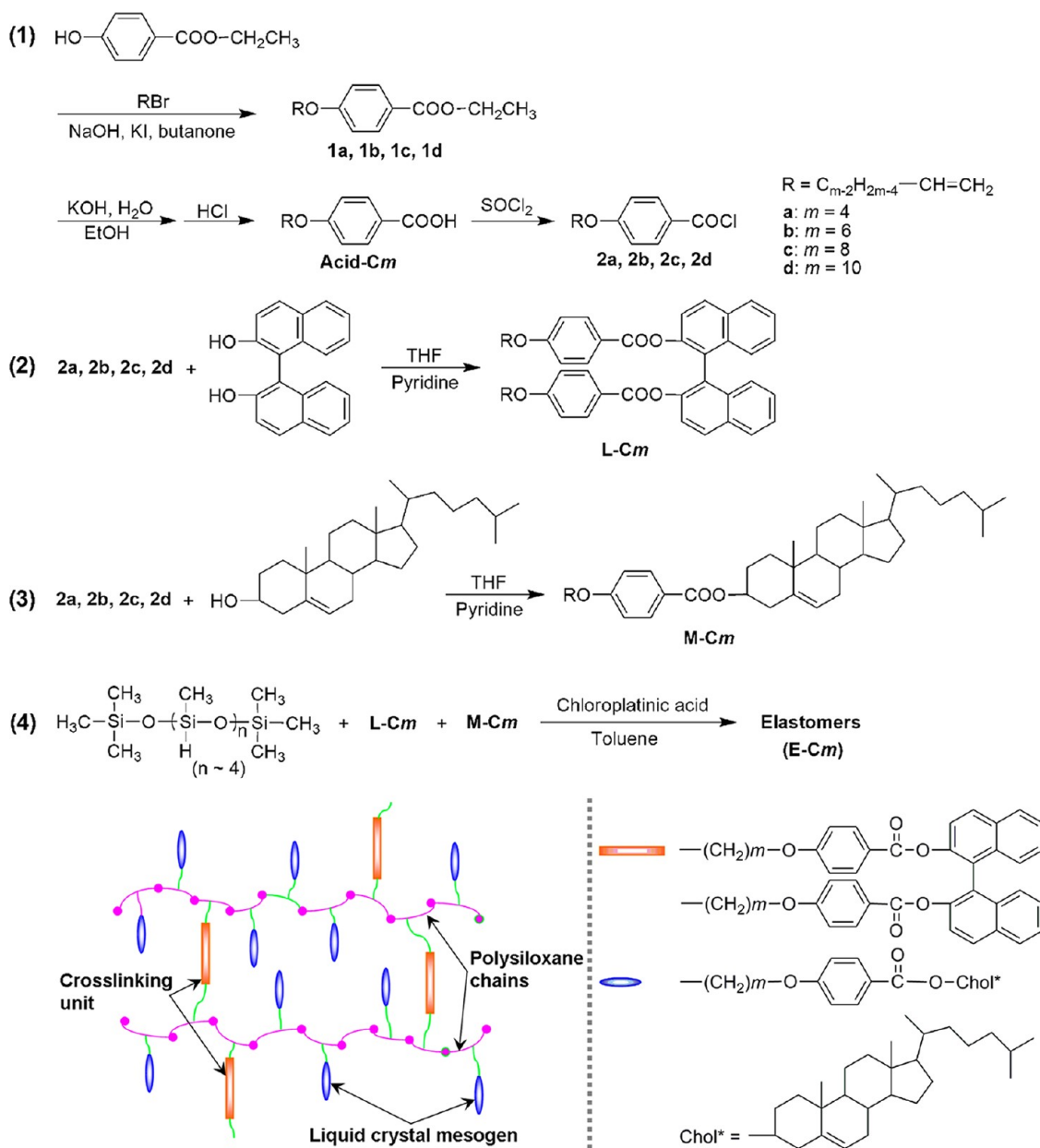
Synthesis of 4-(Dec-9-enyloxy)benzoic Acid, Acid-C10. 10-Bromodec-1-ene (55.0 mmol, 12.05 g) was added dropwise to a mixture of ethyl 4-hydroxybenzoate (50.0 mmol, 8.30 g), 100 mL of butanone, NaOH (55.0 mmol, 2.20 g), and KI (1.00 g) at room temperature and heated to $85\text{ }^\circ\text{C}$ under magnetic stirred for 16 h. After filtration and removal of solvent, the residue was dissolved in 500 mL of 10% NaOH and extracted twice by ether. After removal of ether, 4-(dec-9-enyloxy)phenyl propionate ethyl (**1d**) was obtained. Then, a solution of 300 mL of water and 20.00 g KOH were added to an ethanol (50 mL) solution of **1d** at room temperature. The mixture was heated to $110\text{ }^\circ\text{C}$, refluxed for 10 h, and acidified to pH 3.0 with hydrochloric acid. After filtration, the residue was recrystallized from ethanol to give Acid-C10 as a white crystal. Yield: 12.70 g (92%). FT-IR (KBr, cm^{-1}): 2934–2852 ($-CH_2-$, $CH_2=$ and $=CH$), 2663–2558 ($-OH$ in $-COOH$), 1688 ($C=O$), 1607, 1514 (Ar-), 1258 ($C-O-C$). 1H NMR (300 MHz, $CDCl_3$, TMS, δ , ppm): 8.04–8.02 (d, 2H, $J = 6.3\text{ Hz}$, Ar-H), 6.92–6.90 (d, 2H, $J = 6.3\text{ Hz}$, Ar-H), 5.83–5.76 (m, 1H, $CH_2=CH-$), 5.00–4.90 (m, 2H, $CH_2=CH-$), 4.02–3.98 (t, 2H, $J = 4.8\text{ Hz}$, CH_2-CH_2O-), 2.05–2.00 (q, 2H, $J = 4.8\text{ Hz}$, $=CH-CH_2-$), 1.82–1.75 (m, 2H, CH_2-CH_2O-), 1.44–1.41 (t, 2H, $J = 5.4\text{ Hz}$, $-CH_2-$), 1.31 (s, 8H, $-CH_2-$).

Compounds Acid-C4, Acid-C6, and Acid-C8 were similarly prepared as mentioned for Acid-C10.

4-(But-3-enyloxy)benzoic Acid, Acid-C4. FT-IR (KBr, cm^{-1}) 3025–2817 ($-CH_2-$, $CH_2=$ and $=CH$), 2678–2564 ($-OH$ in $-COOH$), 1678 ($C=O$), 1604, 1577, 1511 (Ar-), 1250 ($C-O-C$). 1H NMR (300 MHz, $CDCl_3$, TMS, δ , ppm): 8.05–8.03 (d, 2H, $J = 6.3\text{ Hz}$, Ar-H), 6.93–6.91 (d, 2H, $J = 6.3\text{ Hz}$, Ar-H), 5.94–5.84 (m, 1H, $CH_2=CH-$), 5.19–5.10 (m, 2H, $CH_2=CH-$), 4.09–4.05 (t, 2H, $J = 5.1\text{ Hz}$, $=CH-CH_2O-$), 2.58–2.53 (q, 2H, $J = 5.1\text{ Hz}$, $-CH_2-$).

4-(Hex-5-enyloxy)benzoic Acid, Acid-C6. FT-IR (KBr, cm^{-1}) 3082–2850 ($-CH_2-$, $CH_2=$ and $=CH$), 2672–2547 ($-OH$ in $-COOH$), 1689 ($C=O$), 1603, 1511 (Ar-), 1255 ($C-O-C$). 1H NMR (300 MHz, $CDCl_3$, TMS, δ , ppm): 8.03 (s, 2H, Ar-H), 6.90 (s, 2H, Ar-H), 5.82–5.78 (t, 1H, $J = 5.1\text{ Hz}$, $CH_2=CH-$), 5.04–4.96 (t, 2H, $J = 7.2\text{ Hz}$, $CH_2=CH-$), 4.02–4.00 (d, 2H, $J = 3.9\text{ Hz}$, CH_2-

Scheme 1. (a) Synthetic Routes of the Crosslinkings and the Liquid Crystalline Monomers; (b) Synthetic Route and Schematic Representation of Elastomers



CH_2O-), 2.11 (s, 2H, $=CH-CH_2-$), 1.80 (s, 2H, CH_2-CH_2O-), 1.57 (s, 2H, $-CH_2-$).

4-(Oct-7-enyloxy)benzoic Acid, Acid-C8. FT-IR (KBr, cm^{-1}): 2924–2851 ($-CH_2-$, $CH_2=$ and $=CH$), 2672–2547 ($-OH$ in $-COOH$), 1690 ($C=O$), 1606, 1513 (Ar-), 1251 ($C-O-C$). 1H NMR (300 MHz, $CDCl_3$, TMS, δ , ppm): 8.04–8.02 (d, 2H, $J = 6.3$ Hz, Ar-H), 6.92–6.90 (d, 2H, $J = 6.6$ Hz, Ar-H), 5.81–5.79 (m, 1H, $CH_2=CH-$), 5.01–4.91 (m, 2H, $CH_2=CH-$), 4.02–3.99 (t, 2H, $J = 4.8$ Hz, CH_2-CH_2O-), 2.07–2.02 (q, 2H, $J = 4.8$ Hz, $=CH-CH_2-$), 1.83–1.76 (m, 2H, CH_2-CH_2O-), 1.46–1.24 (m, 6H, $-CH_2-$).

Synthesis of 4-(Dec-9-enyloxy)benzoyl Chloride, 2d. Acid-C10 (21.0 mmol, 5.80 g) and thionyl chloride (45.0 mmol, 5.36 g) were added into a round flask equipped with an absorption instrument of hydrogen chloride. The mixture was heated to 90 °C and refluxed for 6 h. After removal of the solvent, 2d was obtained and stored hermetically until further reactions.

Synthesis of 1,1'-Binaphthyl-2,2'-diyl Bis(4-(dec-9-enyloxy)benzoate), L-C10. 1,1'-Binaphthyl-2,2'-diol (5.0 mmol, 1.43 g) and pyridine (1.0 mL) were dissolved in dry THF (50 mL) to form a

solution. The solution was added dropwise to 2d (11.0 mmol, 3.20 g), heated to 90 °C, and refluxed for 10 h. The mixture was cooled, filtered, poured in 200 mL of cold water, and extracted twice by CH_2Cl_2 . After removal of the solvent, the residue was purified by column chromatography (silica gel, ethyl acetate/petroleum ether = 3/2) to obtain L-C10. Yield: 2.41 g (60%). FT-IR (KBr, cm^{-1}): 3063, 2928, 2854 ($-CH_2-$, $CH_2=$ and $=CH$), 1779, 1733 ($C=O$), 1641 ($CH=CH_2$), 1604, 1511 (Ar-), 1251 ($-C-O-Ar$), 1159 ($C-O-C$). 1H NMR (300 MHz, $CDCl_3$, TMS, δ , ppm): 8.08–8.06 (d, 2H, $J = 6.6$ Hz, Ar-H), 7.99–7.93 (m, 2H, Ar-H), 7.79–7.24 (m, 10H, Ar-H), 6.93–6.92 (d, 2H, $J = 4.2$ Hz, Ar-H), 6.70–6.68 (d, 4H, $J = 6.6$ Hz, Ar-H), 5.82–5.76 (m, 2H, $CH_2=CH-$), 5.00–4.90 (m, 4H, $CH_2=CH-$), 4.02–3.98 (t, 2H, $J = 5.1$ Hz, CH_2-CH_2O-), 3.91–3.87 (t, 2H, $J = 4.8$ Hz, CH_2-CH_2O-), 2.03–1.99 (t, 4H, $J = 6.0$ Hz, $=CH-CH_2-$), 1.78–1.68 (m, 4H, $-CH_2-$), 1.37–1.22 (m, 20H, $-CH_2-$).

Crosslinkings L-C4, L-C6, and L-C8 were synthesized using the same method as mentioned for L-C10.

1.1'-Binaphthyl-2,2'-diyl Bis(4-(but-3-enyloxy)benzoate), L-C4. FT-IR (KBr, cm^{-1}): 3063, 2948, 2861 ($-\text{CH}_2-$, $\text{CH}_2=$ and $=\text{CH}$), 1733 ($\text{C}=\text{O}$), 1643 ($\text{CH}=\text{CH}_2$), 1606, 1514 (Ar-), 1250 (C-O-Ar), 1167 (C-O-C). ^1H NMR (300 MHz, CDCl_3 , TMS, δ , ppm): 8.10–8.08 (d, 2H, $J = 6.3$ Hz, Ar-H), 7.95–7.93 (d, 2H, $J = 6.6$ Hz, Ar-H), 7.89–7.87 (d, 2H, $J = 6.3$ Hz, Ar-H), 7.78–7.76 (d, 2H, $J = 6.6$ Hz, Ar-H), 7.62–7.31 (m, 8H, Ar-H), 6.70–6.68 (d, 4H, $J = 6.3$ Hz, Ar-H), 5.88–5.78 (m, 2H, $\text{CH}_2=\text{CH}-$), 5.15–5.97 (m, 4H, $\text{CH}_2=\text{CH}-$), 3.97–3.94 (t, 4H, $J = 4.8$ Hz, $\text{CH}_2-\text{CH}_2\text{O}-$), 2.57–2.46 (m, 4H, $=\text{CH}-\text{CH}_2-$).

1.1'-Binaphthyl-2,2'-diyl Bis(4-(hex-5-enyloxy)benzoate), L-C6. FT-IR (KBr, cm^{-1}): 3063, 2942, 2874 ($-\text{CH}_2-$, $\text{CH}_2=$ and $=\text{CH}$), 1778, 1732 ($\text{C}=\text{O}$), 1641 ($\text{CH}=\text{CH}_2$), 1605, 1511 (Ar-), 1251 (C-O-Ar), 1167 (C-O-C). ^1H NMR (300 MHz, CDCl_3 , TMS, δ , ppm): 8.10–8.08 (d, 2H, $J = 6.3$ Hz, Ar-H), 8.06 (m, 2H, Ar-H), 7.98–6.93 (m, 14H, Ar-H), 6.70–6.67 (d, 2H, $J = 6.6$ Hz, Ar-H), 5.80–5.78 (m, 2H, $\text{CH}_2=\text{CH}-$), 5.03–4.94 (m, 4H, $\text{CH}_2=\text{CH}-$), 4.05–4.00 (m, 2H, $\text{CH}_2-\text{CH}_2\text{O}-$), 3.94–3.89 (m, 2H, $\text{CH}_2-\text{CH}_2\text{O}-$), 2.15–2.06 (m, 4H, $=\text{CH}-\text{CH}_2-$), 1.83–1.73 (m, 4H, $-\text{CH}_2-$), 1.59–1.49 (m, 4H, $-\text{CH}_2-$).

1.1'-Binaphthyl-2,2'-diyl Bis(4-(oct-7-enyloxy)benzoate), L-C8. FT-IR (KBr, cm^{-1}): 3061, 2933, 2856 ($-\text{CH}_2-$, $\text{CH}_2=$ and $=\text{CH}$), 1777, 1733 ($\text{C}=\text{O}$), 1641 ($\text{CH}=\text{CH}_2$), 1604, 1512 (Ar-), 1251 (C-O-Ar), 1166 (C-O-C). ^1H NMR (300 MHz, CDCl_3 , TMS, δ , ppm): 8.10–8.08 (d, 2H, $J = 6.9$ Hz, Ar-H), 8.00–7.93 (m, 2H, Ar-H), 7.79–7.76 (t, 2H, $J = 2.7$ Hz, Ar-H), 7.62–7.60 (d, 2H, $J = 6.3$ Hz, Ar-H), 7.52–7.50 (d, 2H, $J = 6.3$ Hz, Ar-H), 7.36–7.22 (m, 4H, Ar-H), 6.95–6.90 (q, 2H, $J = 6.6$ Hz, Ar-H), 6.70–6.68 (d, 4H, $J = 6.3$ Hz, Ar-H), 5.82–5.75 (m, 2H, $\text{CH}_2=\text{CH}-$), 5.00–4.91 (m, 4H, $\text{CH}_2=\text{CH}-$), 4.04–3.98 (q, 2H, $J = 5.1$ Hz, $\text{CH}_2-\text{CH}_2\text{O}-$), 3.91–3.89 (t, 2H, $J = 4.8$ Hz, $\text{CH}_2-\text{CH}_2\text{O}-$), 2.06–2.01 (m, 4H, $=\text{CH}-\text{CH}_2-$), 1.72–1.69 (t, 4H, $J = 4.8$ Hz, $-\text{CH}_2-$), 1.40–1.22 (m, 12H, $-\text{CH}_2-$).

Synthesis of Cholesteryl-4-(dec-9-enyloxy)benzoate, M-C10. Cholesterol (10.0 mmol, 3.86 g) and pyridine (1.0 mL) were dissolved in dry THF (50 mL) to form a solution. The solution was added dropwise to **2d** (11.0 mmol, 3.20 g), heated to 90 °C, and refluxed for 10 h. The mixture was cooled, filtered, poured in 200 mL of cold water, and extracted twice by CH_2Cl_2 . After removal of the solvent, the residue was purified by column chromatography (silica gel, ethyl acetate/petroleum ether = 3/2) to obtain **M-C10**. Yield: 4.19 g (65%). FT-IR (KBr, cm^{-1}): 2940, 2853 ($-\text{CH}_3$ and $-\text{CH}_2-$), 1701 ($\text{C}=\text{O}$), 1641 ($\text{CH}=\text{CH}_2$), 1606, 1512, 1467 (Ar-), 1254 (C-O-Ar), 1168 (C-O-C). ^1H NMR (300 MHz, CDCl_3 , TMS, δ , ppm): 7.97–7.95 (d, 2H, $J = 6.6$ Hz, Ar-H), 6.88–6.86 (d, 2H, $J = 6.6$ Hz, Ar-H), 5.84–5.74 (m, 1H, $\text{CH}_2=\text{CH}-$), 5.39 (d, 1H, $J = 2.4$ Hz, $=\text{CH}-$ in cholesteryl), 4.99–4.90 (m, 2H, $\text{CH}_2=\text{CH}-$), 4.81 (m, 1H, $-\text{CH}_2-\text{CHO}-$), 3.99–3.96 (t, 2H, $J = 4.8$ Hz, $-\text{CHO}-\text{CH}_2-$), 2.43–2.41 (d, 2H, $J = 6.0$ Hz, $-\text{CH}_2-$), 2.03–0.85 (m, 46H, $-\text{CH}_2-$, cholesteryl-H), 0.84–0.83 (d, 6H, $J = 1.2$ Hz, $-\text{CH}-\text{CH}_3$), 0.66 (s, 3H, $-\text{CH}-\text{CH}_3$).

Liquid crystalline monomers **M-C4**, **M-C6**, and **M-C8** were synthesized using the same method as mentioned for **M-C10**.

Cholesteryl-4-(but-3-enyloxy)benzoate, M-C4. FT-IR (KBr, cm^{-1}): 2944, 2867 ($-\text{CH}_3$ and $-\text{CH}_2-$), 1711 ($\text{C}=\text{O}$), 1645 ($\text{CH}=\text{CH}_2$), 1608, 1511, 1467 (Ar-), 1252 (C-O-Ar), 1165 (C-O-C). ^1H NMR (300 MHz, CDCl_3 , TMS, δ , ppm): 7.97–7.95 (d, 2H, $J = 6.6$ Hz, Ar-H), 6.89–6.87 (d, 2H, $J = 6.6$ Hz, Ar-H), 6.06–6.03 (m, 1H, $\text{CH}_2=\text{CH}-$), 5.40–5.39 (d, 1H, $J = 3.0$ Hz, $=\text{CH}-$ in cholesteryl), 5.18–5.09 (m, 2H, $\text{CH}_2=\text{CH}-$), 4.06–4.03 (t, 3H, $J = 4.8$ Hz, $-\text{CH}_2-\text{CHO}-$, $-\text{CH}_2-\text{CH}_2\text{O}-$), 2.57–2.52 (q, 2H, $J = 5.1$ Hz, $-\text{CHO}-\text{CH}_2-$), 2.44–2.42 (d, 2H, $J = 6.0$ Hz, $=\text{CH}-\text{CH}_2-$), 2.02–0.67 (m, 41H, cholesteryl-H).

Cholesteryl-4-(hex-5-enyloxy)benzoate, M-C6. FT-IR (KBr, cm^{-1}): 2944, 2868 ($-\text{CH}_3$ and $-\text{CH}_2-$), 1711 ($\text{C}=\text{O}$), 1641 ($\text{CH}=\text{CH}_2$), 1608, 1511, 1466 (Ar-), 1248 (C-O-Ar), 1163 (C-O-C). ^1H NMR (300 MHz, CDCl_3 , TMS, δ , ppm): 7.97–7.95 (d, 2H, $J = 6.6$ Hz, Ar-H), 6.88–6.86 (d, 2H, $J = 6.6$ Hz, Ar-H), 5.82–5.80 (m, 1H, $\text{CH}_2=\text{CH}-$), 5.40–5.39 (d, 1H, $J = 3.0$ Hz, $=\text{CH}-$ in cholesteryl), 5.04–4.95 (m, 2H, $\text{CH}_2=\text{CH}-$), 4.82–4.79 (t, 1H, $J =$

3.6 Hz, $-\text{CH}_2-\text{CHO}-$), 4.01–3.98 (t, 2H, $J = 4.8$ Hz, $-\text{CH}_2-$), 2.44–2.42 (d, 2H, $J = 5.7$ Hz, $-\text{CHO}-\text{CH}_2-$), 2.12–2.10 (d, 2H, $J = 5.4$ Hz, $=\text{CH}-\text{CH}_2-$), 1.87–0.67 (m, 45H, $-\text{CH}_2-\text{CH}_2\text{O}-$, cholesteryl-H).

Cholesteryl-4-(oct-7-enyloxy)benzoate, M-C8. FT-IR (KBr, cm^{-1}): 2946, 2850 ($-\text{CH}_3$ and $-\text{CH}_2-$), 1700 ($\text{C}=\text{O}$), 1641 ($\text{CH}=\text{CH}_2$), 1605, 1512, 1466 (Ar-), 1254 (C-O-Ar), 1171 (C-O-C). ^1H NMR (300 MHz, CDCl_3 , TMS, δ , ppm): 7.97–7.95 (d, 2H, $J = 5.7$ Hz, Ar-H), 6.88–6.86 (d, 2H, $J = 6.0$ Hz, Ar-H), 5.84–5.74 (m, 1H, $\text{CH}_2=\text{CH}-$), 5.39 (s, 1H, $=\text{CH}-$ in cholesteryl), 5.00–4.91 (m, 2H, $\text{CH}_2=\text{CH}-$), 4.81 (m, 1H, $-\text{CH}_2-\text{CHO}-$), 3.99–3.96 (t, 2H, $J = 4.5$ Hz, $-\text{CHO}-\text{CH}_2-$), 2.43–2.41 (d, 2H, $J = 6.0$ Hz, $-\text{CH}_2-$), 2.05–0.90 (m, 42H, $-\text{CH}_2-$, cholesteryl-H), 0.85–0.83 (d, 6H, $J = 4.8$ Hz, $-\text{CH}-\text{CH}_3$), 0.66 (s, 3H, $-\text{CH}-\text{CH}_3$).

Synthesis of Elastomers. All elastomers were synthesized by a one-step hydrosilylation reaction. As the crosslinkings and the mesogenic monomers both have chiral centers with the same handedness in the molecules, the synthesized elastomers are all chiral.⁴⁵ The synthetic route and schematic representation of elastomers are shown in Scheme 1(4). A typical polymerization procedure was carried out as the following, again, using **E-C10** as an example. About 0.15 g (0.19 mmol) of crosslinking agent **L-C10** and 0.73 g (1.14 mmol) of monomer **M-C10** were dissolved in 50 mL of dry, fresh distilled toluene. To the stirred solution, 0.16 g (0.40 mmol) of PMHS and 2 mL of $\text{H}_2\text{PtCl}_6/\text{THF}$ (0.50 g of hexachloroplatinic acid hydrate dissolved in 100 mL of tetrahydrofuran) were added and heated under nitrogen and anhydrous conditions at 110.0 °C for 36 h. After removal of the solvent, the residue was dissolved in THF and precipitated in methanol three times. Finally, the elastomer was dried under vacuum.

Preparation of the Cells. To obtain homogeneous alignment, a 2.0 wt % polyvinyl alcohol (PVA) aqueous solution was coated onto the inner surfaces of the substrates of the cells by spin-casting. The deposited film was dried at 80.0 °C for about 1 h and subsequently rubbed with a textile cloth under a pressure of 2.0 g cm^{-2} along one direction. To induce homeotropic orientation of liquid crystals, the inner surfaces of the substrates were treated with *N,N*-dimethyl-*N*-octadecyl-3-aminopropyltrimethoxysilyl chloride (DMOAP) solution (0.1% by volume in water).⁴⁶ The mechanical effects are very strong in cholesteric elastomers,⁴⁷ and the studied sample was filled into the cell by capillary action in the temperature range of the cholesteric or isotropic phase.

Preparation of the Mixtures. To investigate the influence of the flexible carbon chain length on the helical twisting behaviors of monomers and elastomers, mixtures **1–12** were prepared by doping them into a nematic LC. As the monomers and elastomers are all chiral, mixtures **1–12** were cholesteric liquid crystals and exhibited a cholesteric structure when filling them into a homogeneously treated cell. Mixtures **13** and **14** were prepared to fabricate wide-band reflective films. All the mixtures were obtained by dissolving different components in dichloromethane and evaporating the solvent slowly. The compositions, weight ratios, phase transition temperatures, and corresponding enthalpy changes of these mixtures are listed in Table 1.

Characterization of Helical Twisting Power of Monomers and Elastomers. A CLC can be formed when a nematic LC host is doped with a chiral dopant guest. The pitch of the CLC so obtained, $P = [(\text{HTP})\text{Xc}]^{-1}$, where HTP and Xc are the helical twisting power and molar concentration of the chiral dopant, respectively.⁴⁸ To characterize the twisting power of the synthesized monomers and elastomers, the value P of the CLCs (mixtures **1–12**), induced by doping them in a nematic LC SLC-1717, was used as the weight ratio was fixed in 2 wt %.

The pitch lengths were measured by the Cano-wedge technique.⁴⁹ In this measurement, a wedge-shaped cell (KCRK-07, Japan) with a wedge angle, θ (0.01937 rad), was used and the inner surfaces of its two glass substrates were treated to provide a homogeneous orientation of the LC molecules. After the mixture was filled into the cell, a Grandjean-Cano texture formed with disclination lines separated by a distance D . The pitch length P is determined from $P = 2D \tan \theta \approx 2D\theta$.

Table 1. The Compositions, Weight Ratios, Phase Transition Temperatures, and Corresponding Enthalpy Changes of Mixtures 1–14

mixture (type)	wt ratio (wt %)	$T_{\text{Ch-I}}^c$ (°C)	ΔH (J g ⁻¹) ^d
1	2.0/-/-/-/-/-/-/-/-/-/98.0 ^a	85.3	0.39
2	-/2.0/-/-/-/-/-/-/-/-/98.0 ^a	85.6	0.21
3	-/-/2.0/-/-/-/-/-/-/-/-/98.0 ^a	85.6	0.12
4	-/-/-/2.0/-/-/-/-/-/-/-/-/98.0 ^a	85.1	0.28
5	-/-/-/-/2.0/-/-/-/-/-/-/-/-/98.0 ^a	91.8	0.32
6	-/-/-/-/-/2.0/-/-/-/-/-/-/-/-/98.0 ^a	92.8	0.37
7	-/-/-/-/-/-/2.0/-/-/-/-/-/-/-/-/98.0 ^a	92.6	0.28
8	-/-/-/-/-/-/2.0/-/-/-/-/-/-/-/-/98.0 ^a	91.8	0.23
9	-/-/-/-/-/-/-/2.0/-/-/-/-/-/-/-/-/98.0 ^a	90.4	0.28
10	-/-/-/-/-/-/-/-/2.0/-/-/-/-/-/-/-/-/98.0 ^a	90.7	0.40
11	-/-/-/-/-/-/-/-/-/2.0/-/-/-/-/-/-/-/-/98.0 ^a	90.1	0.81
12	-/-/-/-/-/-/-/-/-/-/2.0/98.0 ^a	90.5	0.39
13	95.98/-/4.0/0.01/0.01 ^b	143.4	0.43
14	-/95.98/4.0/0.01/0.01 ^b	142.2	0.54

^aWeight ratio: L-C4/L-C6/L-C8/L-C10/M-C4/M-C6/M-C8/M-C10/E-C4/E-C6/E-C8/E-C10/SLC-1717. ^bWeight ratio: E-C8/E-C10/C6M/IRG651/DMP. ^c $T_{\text{Ch-I}}$: clearing temperature from cholesteric to isotropic phase. ^d ΔH : Delta H from cholesteric to isotropic phase.

Preparation of the Wide-Band Reflective Films. Mixture 13 or 14 was filled into homogeneous treated cells with different cell thickness (10, 20, 40, 60, or 80 μm) at high temperature below their clearing temperatures. The wide-band reflective cells were prepared by carrying out the following procedure. The cells of mixtures were irradiated with UV light (5 mW cm⁻², 365 nm) for different times (10, 20, 40, 60, or 80 min) at high temperature (115 °C for mixture 13 and 131 °C for mixture 14), during which polymer network was formed from the photopolymerization of C6M. Then they were cooled slowly to low temperature and quenched below their glass transition temperatures.

The samples for SEM studies were prepared as follows. The wide-band reflective cells of the mixtures were plunged in liquid nitrogen and broken in a direction perpendicular to the plates. Then the fractured surfaces of the cells were sputtered with a thin layer of gold and observed.

RESULTS AND DISCUSSION

Synthesis and Characterization of Monomers and Elastomers. As shown in Scheme 1, the monomers were synthesized in four steps. The structures of the monomers were confirmed by FT-IR and ¹H NMR spectroscopic methods. Target elastomers were synthesized by the hydrosilylation of PMHS with the binaphthalene derivatives and cholesterol derivatives using H₂PtCl₆ as the catalyst.

With E-C10 as an example, FT-IR spectra of E-C10, PMHS, L-C10, and M-C10 are shown in Figure 2. The disappearance of the sharp vibrational band at 2164 cm⁻¹, which was assigned as the Si–H stretching, showed that all the Si–H groups were reacted completely. The appearance of the vibrational bands at 2934–2850, 1710, 1605–1470, and 1121–1020 cm⁻¹, which were attributed to vibrations from methylene (–CH₂–), ester carbonyl (C=O), aromatic (Ar–), and Si–O–Si, respectively, illustrated the successful preparation of the elastomer. Additionally, from the partial amplification of the spectra between 1800 and 1500 cm⁻¹ as shown in Figure 2b, it can be found that the vibrational band at 1641 cm⁻¹ corresponding to olefinic C=C stretching disappeared, indicating totally reaction of the monomers.

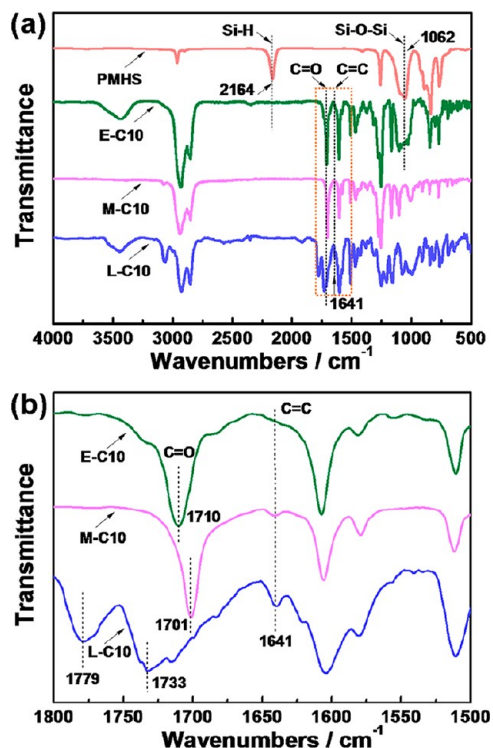
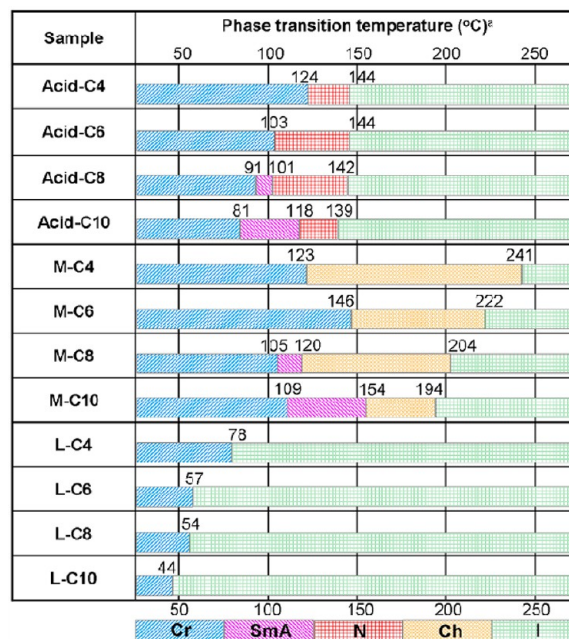


Figure 2. (a) FT-IR spectra of E-C10, PMHS, L-C10, and M-C10; (b) partial amplification of the spectra in (a) between 1800 and 1500 cm⁻¹.

Phase Transitions of Monomers. The thermal properties of the acids and monomers were determined by DSC and POM measurements, which data are summarized in Figure 3. Acid-C8 and Acid-C10 showed smectic A (SmA) and nematic (N) phases, but Acid-C4 and Acid-C6 showed only N phase in the heating process. M-C8 and M-C10 showed SmA and Ch



^a Cr: crystal, SmA: smectic A, N: nematic, Ch: cholesteric, I: isotropic.

Figure 3. Phase transition temperatures of the acids, liquid crystalline monomers, and crosslinkings.

Table 2. Thermal Properties of Elastomers E-Cm

elastomers	DSC			POM		
	T_g^a (°C)	T_m^a (°C)	T_i^a (°C)	transition temperature ^b (°C)	ΔT^c (°C)	T_d^d (°C)
E-C4	52.3 (0.40)	109.0 (16.37)	162.6 (0.97)	G 110.0 Ch 164.0 I G 99.0 Ch 154.0 I	53.6	305
E-C6	42.1 (0.80)	116.2 (14.25)	162.7 (0.71)	G 118.0 Ch 165.0 I G 110.0 Ch 156.0 I	46.5	312
E-C8	42.4 (1.24)	110.4 (13.89)	152.6 (0.73)	G 114.0 Ch 154.0 I G 90.0 Ch 127.0 BP 144.1 I	42.2	270
E-C10	56.1 (2.52)	89.3 (6.53)	151.6 (0.84)	G 90.0 SmA 140.0 Ch 152.0 I G 65.0 SmA 135.4 Ch 143.8 BP 146.1 I	62.3	261

^aEvaluated by DSC at a rate of 10 °C/min. The data in the parentheses are the corresponding enthalpy changes (ΔH in $J g^{-1}$). ^bEvaluated by POM measurement during heating (the up row) and cooling (the down row) processes. G, glassy; Ch, cholesteric phase; I, isotropic phase; SmA, smectic A phase; BP, blue phase. ^cMesophase temperature ranges from DSC measurement. ^dThe temperature at which 5% weight loss of the sample from TGA under nitrogen atmosphere at a heating rate of 10 °C/min.

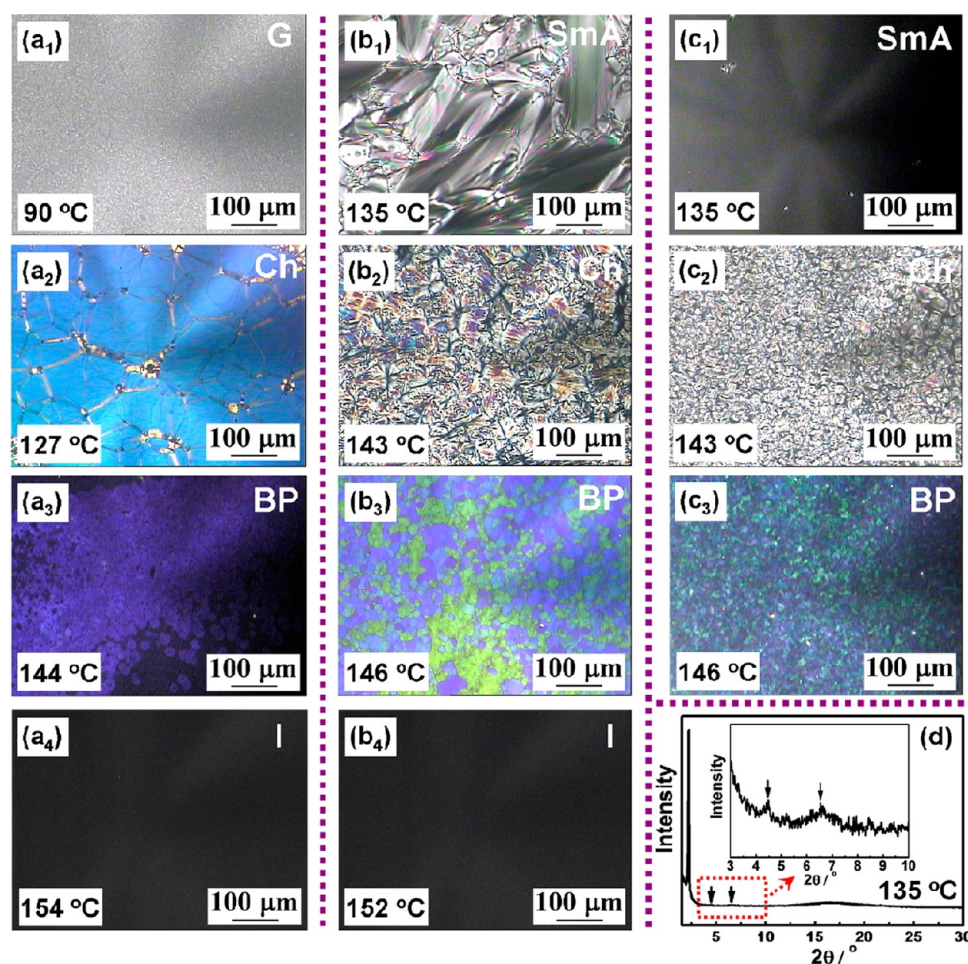


Figure 4. Optical textures of E-C8 and E-C10 when cooled from their isotropic states. No birefringence of glassy at 90 °C (a₁), planar texture of Ch phase at 127 °C (a₂), BP texture at 144 °C (a₃) and isotropic state at 154 °C (a₄) for E-C8 in a homogeneously treated cell; fan-shaped texture of SmA phase at 135 °C (b₁), cholesteric phase texture at 143 °C (b₂), BP texture at 146 °C (b₃) and isotropic state at 152 °C (b₄) for E-C10 in a homogeneously treated cell; pseudoisotropic texture of SmA phase at 135 °C (c₁), focal-conic texture of Ch phase at 143 °C (c₂) and BP texture at 146 °C (c₃) for E-C10 in a homeotropically treated cell, respectively. (d) The 1D WAXD pattern of E-C10 at 135 °C during a cooling process. The inset is partial amplification of the pattern between 3 and 10°.

phases, while M-C4 and M-C6 showed only Ch phase in the heating process. In other words, increase of the terminal alkenyl chain length helps to the formation of SmA phase. Crosslinking

agent L-Cm shows no liquid crystalline phases during both heating and cooling processes because of their nonlinear structure. Besides, the clearing or melting temperature of acids

and monomers decreased with increasing alkenyl chain length due to the increased flexibility by the alkenyl end chains.

Phase Transitions and Phase Structures of the Elastomers. The phase behaviors of all the elastomers were investigated by DSC and POM measurements. The thermal properties of these elastomers, which are dependent on the number of carbon atoms in the interim alkyl groups, m , for the E- Cm series, are listed in Table 2.

As shown in Table 2, the temperatures at 5% weight loss under N_2 (T_{d5}) were all over 260 °C, indicating that all the elastomers had good thermal stabilities. From DSC measurement, a glass transition temperature (T_g), a melting transition temperature (T_m), and a clearing temperature (T_i) can be detected in the curves of all the synthesized elastomers. T_i decreased with increasing interim alkyl chain length from E-C4 to E-C10 due to the increased plasticization by the alkyl chains. All the elastomers have wide mesophase temperature ranges as summarized in Table 2.

To confirm the liquid crystalline phase transitions, all the elastomers were observed by POM measurement. During T_m and T_i , E-C4 and E-C6 showed Ch phase textures in both the heating and cooling processes. E-C8 showed Ch phase in the heating process but blue phase (BP) and Ch phase in the cooling process. Worthily, E-C10 showed smectic (Sm) and Ch phases in a heating process, and BP, Ch, and Sm phases in the cooling process. Figure 4 shows the POM photographs of E-C8 and E-C10 when cooling from their isotropic states. When the elastomer was filled into a homogeneously treated cell above its clearing temperature, it showed a black field corresponding to isotropic state (Figure 4a₄,b₄). As cooling, E-C8 exhibited subsequently blue phase texture (Figure 4a₃), planar texture for Ch phase (Figure 4a₂), and then turned glassy below 90 °C, presenting no texture and birefringence as shown in Figure 4a₁. Different from E-C8, E-C10 showed fan-shaped texture corresponding to Sm phase (Figure 4b₁), after its BP texture (Figure 4b₃) and Ch phase texture (Figure 4b₂).

To identify the kind of Sm phase for E-C10, it was filled into a homeotropically treated cell. In a cooling process, it exhibited a black field for isotropic state, BP texture (Figure 4c₃), and focal conic texture containing orderly fingerprint texture for the Ch phase (Figure 4c₂). Subsequently, it showed a black field (Figure 4c₁) again, which is the characteristic of SmA or SmB phase. In the 1D WAXD pattern of E-C10 at 135 °C, a sharp peak at $2\theta = 2.26^\circ$ and equidistant diffractions in the small-angle region emerge along with a broad and unobscured halo centering at $2\theta \approx 17^\circ$ in the wide-angle region (Figure 4d). As the appearance of a single sharp diffraction at the wide-angle region is necessary to indicate the existence of SmB phase,⁵⁰ we rule out the possibility of a SmB phase. Combined with the results of Figure 4b₁,c₁, the Sm phase of E-C10 could be determined to be a SmA phase. In conclusion, the increase of the interim alkyl chain length contributes to the formation of SmA phase and blue phase for the elastomers.

Helical Twisting Behaviors of Monomers and Elastomers. Figure 5 shows the temperature dependence of the pitch lengths of mixtures 1–4, 5–8, and 9–12, respectively. It can be seen that the crosslinkings L- Cm or monomers M- Cm with different terminal alkenyl chain length exhibit a similar temperature dependence of HTP. For example, P increases for mixtures 1–4, decreases for mixtures 5–8 with increasing temperature as shown in parts a and b of Figure 5. But it should be noted that L- Cm and M- Cm have opposite temperature dependence of HTP. Furthermore, the values of P increase first

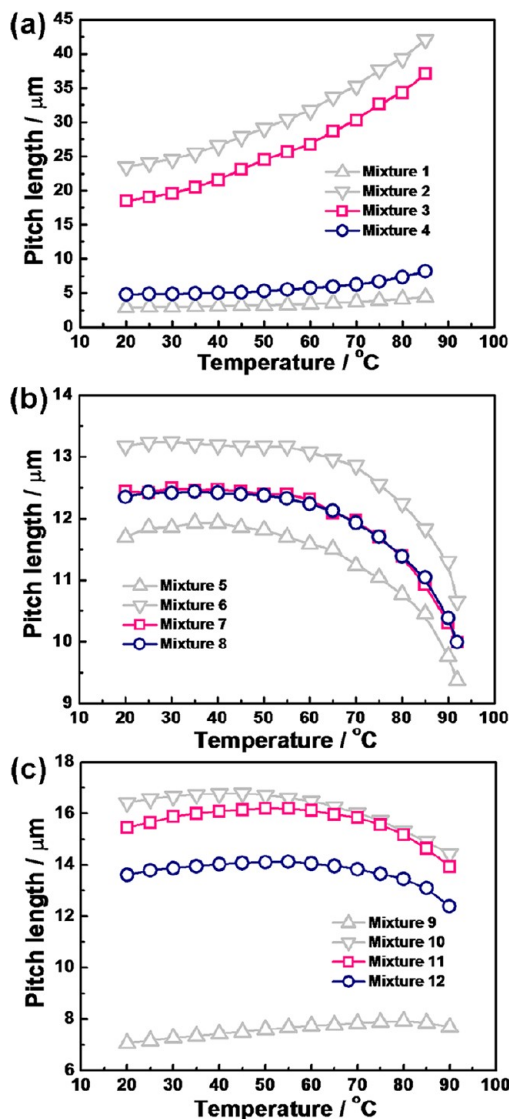


Figure 5. Temperature dependence of the pitch lengths of mixtures 1–4 (a), mixtures 5–8 (b), and mixtures 9–12 (c).

and then decrease with increasing terminal alkenyl chain length. Typically, the P values at 20 °C were 2.9 μm for mixture 1, 23.5 μm for mixture 2, 18.5 μm for mixture 3, and 4.8 μm for mixture 4, respectively. It was found that the twisting power is weakly dependent on the nature of the aliphatic chiral center,^{51,52} the decreasing or increasing HTP values (increasing or decreasing P values) with increasing terminal alkenyl chain length from 4 to 10, may result from smaller or greater anisometry of molecular structure.

The HTP of elastomers grafting both L- Cm and M- Cm exhibited a turning point with increasing temperature due to the coordination of the crosslinkings and the liquid crystalline monomers. For instance, the pitch length of mixture 11 increases from 15.5 to 16.2 μm with increasing temperature from 20 to 50 °C, while it decreases to 13.9 μm when increasing temperature continuously to 90 °C as shown in Figure 5c. The turning point extrapolated from the P values were 80 °C for E-C4, 45 °C for E-C6, 50 °C for E-C8, and 55 °C for E-C10, respectively. Besides, the HTP decreases first and then increases with increasing interim alkyl chain length from 4 to 10 following the same rule as to the monomers.

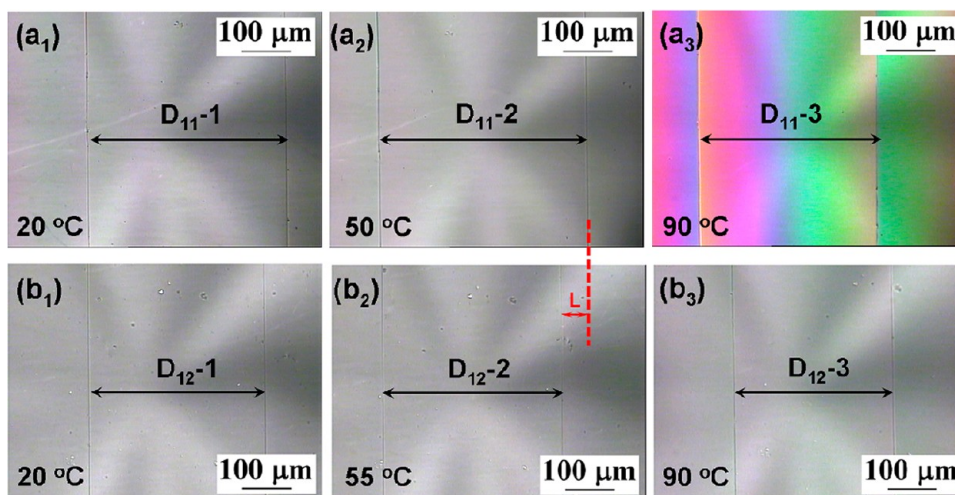


Figure 6. POM micrographs of mixtures 11 and 12 at different temperature in wedge-shaped cells: mixture 11 at 20 °C (a₁), 50 °C (a₂) and 90 °C (a₃), $D_{11-3} < D_{11-1} < D_{11-2}$; mixture 12 at 20 °C (b₁), 55 °C (b₂) and 90 °C (b₃), $D_{12-3} < D_{12-1} < D_{12-2}$, respectively.

Typically, the HTP of E-C10 is larger than that of E-C8. Correspondingly, the pitch length of mixture 12 is smaller than that of mixture 11 as shown in Figure 6. Taking the pitch length at their turning point as an example, the distance of parallel disclination lines in Figure 6b₂ is L narrower than that in Figure 6a₂. In conclusion, the interim alkyl chain length in the synthesized elastomers has a great influence on their helical twisting behaviors.

Application of Elastomers in Visible and Near-Infrared Wide-Band Reflective Films. Figure 7 shows the

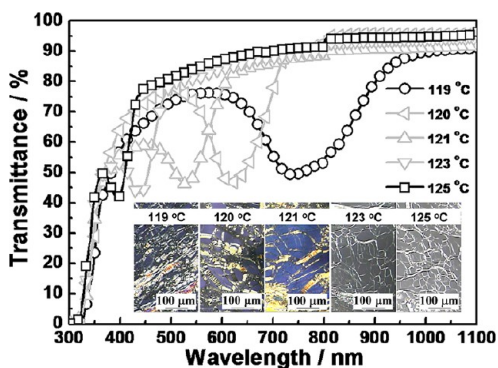


Figure 7. The transmission spectra of E-C8 at different temperature and the POM photographs corresponding to temperature.

transmission spectra of E-C8 at different temperature. It can be found that the reflection wavelength becomes shorter with increasing temperature, and is located in 752, 621, 527, 435, and 396 nm at 119, 120, 121, 123, and 125 °C, respectively. This is due to that the HTP of E-C8 increases with increasing temperature above its turning point 50 °C. Worthily, it remained good planar texture with the increase of temperature from 119 to 125 °C as shown in the inset of Figure 7, which ensured the high reflective intensity.

To fabricate wide-band reflective films, mixture 13 containing LCEs without SmA phase and mixture 14 containing LCEs with SmA phase were prepared. Figure 8a shows the transmission spectra of mixtures 13 and 14 before and after UV curing for 40 min in the cells with 40 μm thickness. It can be seen that the bandwidth of the spectra become broadened

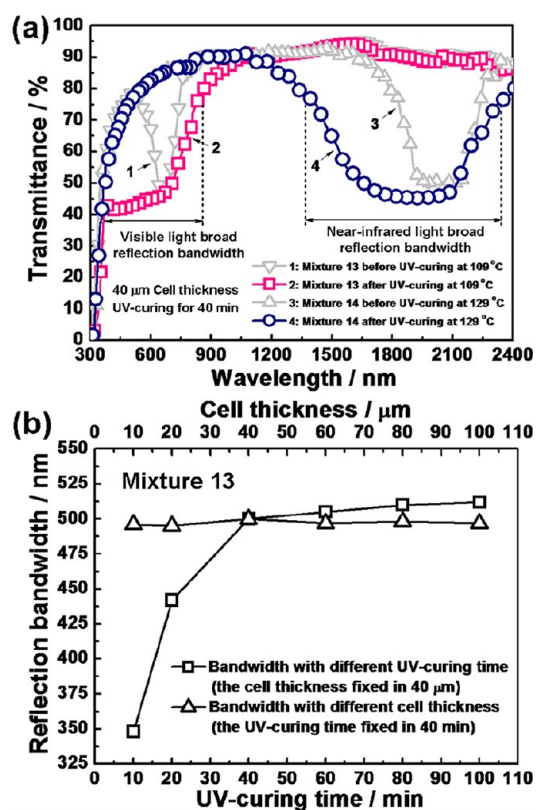


Figure 8. (a) The transmission spectra of mixtures 13 and 14 before and after UV curing for 40 min in the cells with 40 μm thickness; (b) UV curing time and cell thickness dependence of the reflection bandwidth for mixture 13 after polymerization.

after UV curing. Mixture 13 reflects the visible light flux range of 350–850 nm after polymerization at 109 °C (curve 2). The center reflection wavelength of mixture 14 locates in 2055 nm at 129 °C before UV curing (curve 3). And the reflection band broadened to 970 nm in the near-infrared light flux range of 1370–2340 nm after polymerization (curve 4). In other words, visible and near-infrared wide-band reflective films can be obtained from E-C8 and E-C10 by blending with a small quantity of photopolymerizable monomers, respectively.

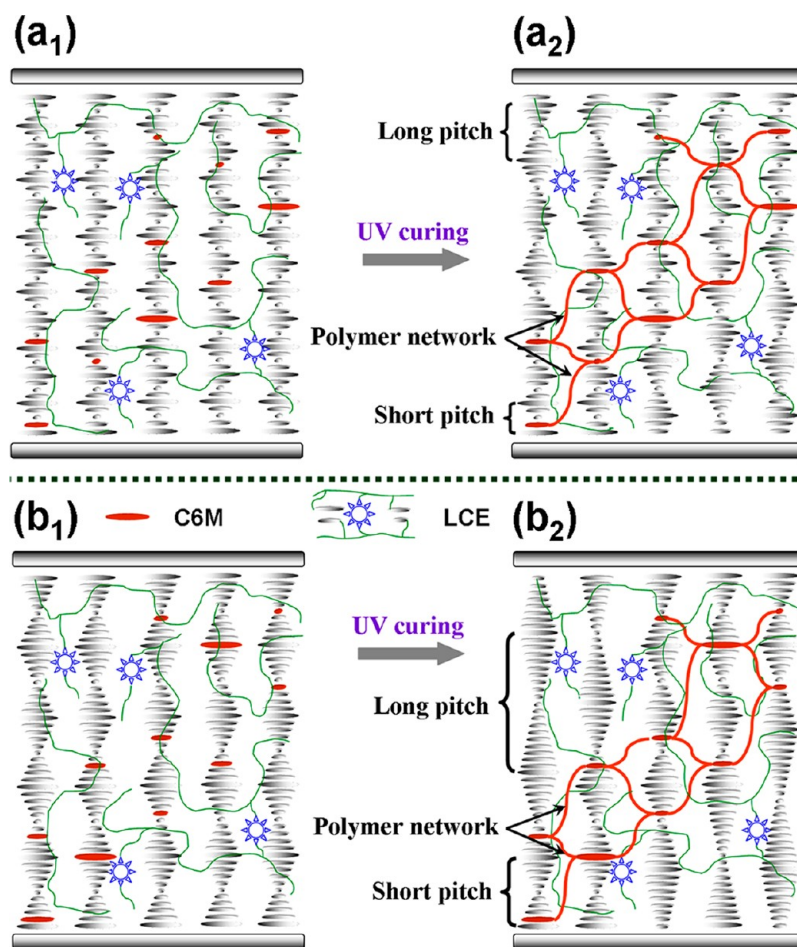


Figure 9. The schematic representation of LCE molecules in the cell containing mixture 13 (a_1 and a_2) or mixture 14 (b_1 and b_2) when temperature changes: before UV curing at high temperature (a_1 and b_1) and after UV curing at low temperature (a_2 and b_2).

Then we investigated the influence of the UV curing time and the cell thickness on the optical properties of the wide-band reflective films. Figure 8b shows the UV curing time and cell thickness dependence of the reflection bandwidth for mixture 13 after polymerization. It can be seen that the reflection bandwidth increases obviously with increasing UV curing time from 10 to 40 min, while it tends to be stable after 40 min even when increase in the UV curing time continued. In addition, it changes little with different cell thickness from 10 to 100 μm as shown in Figure 8b.

A conceivable explanation to above phenomenon is given considering the change of pitch length in synthesized elastomers when temperature changes and the anchoring effect of the polymer network. Figure 9a shows the schematic representation of the rearrangement of the LCE molecules in mixture 13 when temperature changes. At high temperature, it was filled into a homogeneously treated cell and exhibited uniform short pitch as shown in Figure 9a₁. Then this short pitch was fixed in some local regions surrounded by the polymer network formed from the photopolymerization of C6M after UV curing. As the HTP of E-C8 increased with the increase of temperature above its turning point, its pitch length had a tendency to decrease as the temperature rose. So when cooling, the pitch length of mixture 13 became long in some other regions, where the anchoring effect of the polymer network was not enough to prevent the LCE molecules from rearranging, as shown in Figure 9a₂. Different from mixture 13,

mixture 14 was filled into the cell at a temperature a little above its SmA-Ch phase transition temperature and exhibited uniform pitch larger than that of mixture 13 as shown in Figure 9b₁. When cooling, it tended to change to be SmA phase in the regions with weak anchoring effect of the polymer network, and the pitch length became longer correspondingly, as shown in Figure 9b₂. Finally, benefiting from the polymer property hold by the LCEs, the longer pitch can be frozen after quenching cells below their glass transition temperatures. As a result, small and large nonuniform pitch distributions are formed in mixture 13 and mixture 14, as shown in parts a₂ and b₂ of Figure 9, respectively.

It is well-known that the polymerization of the photopolymerizable monomer proceeds gradually with increasing UV curing time and stops when the monomer is exhausted. As the concentration of the monomer C6M in mixtures 13 and 14 is fixed, the anchoring effect of the polymer network, which contributes to the fixation of the short pitch, increases first and then changes little with the increase of UV curing time. Correspondingly, the reflection bandwidth of the mixtures after polymerization increases first and then tends to be stable with increasing UV curing time. Besides, as the nonuniform pitch distributions are formed under certain UV intensity, the reflection bandwidth is scarcely influenced by the cell thickness.

To demonstrate the mechanism described above, nonuniform pitch distributions of mixtures 13 and 14 after UV curing for 40 min in the cells with 40 μm thickness were observed with

a scanning electron microscopy (SEM). Parts a and b of Figure 10 show SEM images of the fractured surfaces of the irradiated

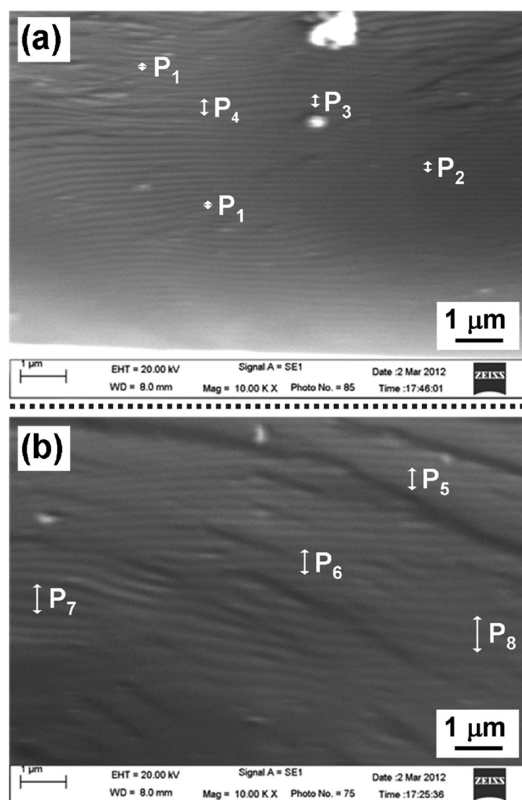


Figure 10. SEM photographs of the fractured surfaces of mixture 13 (a) and mixture 14 (b). The dimension of the bands in the fine structure on the fractured planes corresponds to a π molecular rotation, that is, $P/2$. There is a small nonuniform pitch distribution in mixture 13, $P_1 < P_2 < P_3 < P_4$; a large nonuniform pitch distribution in mixture 14, $P_5 < P_6 < P_7 < P_8$.

cells. The dimension of the two bands in the fine structure on the fractured planes corresponds to a π molecular rotation, that is, $P/2$. It can be seen that different pitch lengths distributed randomly in the fractured plane. For example, pitch lengths from about $0.15 \mu\text{m}$ (P_1) to $0.36 \mu\text{m}$ (P_4) distributed randomly in the fractured plane of the irradiated cell containing mixture 13 as shown in Figure 10a, from about $0.54 \mu\text{m}$ (P_5) to $0.93 \mu\text{m}$ (P_8) allocated irregularly in that of the cell containing mixture 14 as shown in Figure 10b. According to the equation $\lambda = nP$, λ_1 should be 350 nm while λ_4 should be 850 nm in theory, which almost covers the visible light region. Similarly, λ_5 should be 1370 nm and λ_8 should be 2340 nm in theory, which nearly mantles the near-infrared light region. This demonstrates that mechanism explained above is reasonable. By adjusting the interim alkyl chain length in the elastomers, both visible and near-infrared light wide-band reflective films can be obtained.

CONCLUSIONS

In summary, a series of side-chain LCEs with binaphthalene derivatives as crosslinkings based on polysiloxane were synthesized and characterized. The phase transition temperatures, helical twisting behaviors, and reflective behaviors of the elastomers were investigated. The elastomers with short interim alkyl chain length, E-C4, E-C6, and E-C8, formed Ch phases, while E-C10 with longer interim alkyl chain length formed Ch

and SmA phases. In addition, E-C8 and E-C10 can form blue phases under a cooling process. The results show that the interim alkyl chain length has a great influence on the helical twisting behaviors of the elastomers, and visible or near-infrared light wide-band reflective films can be obtained by utilizing elastomers with short or long interim alkyl chain length, respectively. These broadband reflective films have practical applications in visible brightness enhancement films and IR shielding films.

AUTHOR INFORMATION

Corresponding Author

*E-mail: yanghuai@mater.ustb.edu.cn.

Notes

The authors declare no competing financial interest.

ACKNOWLEDGMENTS

This work was supported by National Natural Science Fund for Distinguished Yong Scholar (grant no. 51025313), National Natural Science Foundation (grant no. 50973010 and 51173003), Open Research Fund of State Key Laboratory of Bioelectronics (Southeast University), the Fundamental Research Funds for the Central Universities (grant no. FRF-TP-12-032A) and National Natural Science Foundation (grant no. 51143001).

REFERENCES

- (1) Finkelmann, H.; Rehage, G. In *Liquid Crystal Polymers*; Academic Press: New York, 1984; pp 99–172.
- (2) Urayama, K. *Macromolecules* **2007**, *40*, 2277–2288.
- (3) Brand, H. R.; Pleiner, H.; Martinoty, P. *Soft Matter* **2006**, *2*, 182–189.
- (4) Sawa, Y.; Ye, F.; Urayama, K.; Takigawa, T.; Gimenez-Pinto, V.; Selinger, R. L. B. *Proc. Natl. Acad. Sci. U.S.A.* **2011**, *108*, 6364–6368.
- (5) Serra, F.; Matranga, M. A.; Ji, Y.; Terentjev, E. M. *Opt. Express* **2010**, *18*, 575–581.
- (6) Menzel, A. M.; Pleiner, H.; Brand, H. R. *J. Chem. Phys.* **2007**, *126*, 234901.
- (7) Beyer, P.; Zentel, R. *Macromol. Rapid Commun.* **2005**, *26*, 874–879.
- (8) Ji, Y.; Huang, Y. Y.; Terentjev, E. M. *Langmuir* **2011**, *27*, 13254–13260.
- (9) Sanchez-Ferrer, A.; Finkelmann, H. *Solid State Sci.* **2010**, *12*, 1849–1852.
- (10) Biggins, J. S.; Warner, M.; Bhattacharya, K. *J. Mech. Phys. Solids* **2012**, *60*, 573–590.
- (11) Yamazaki, H.; Takeda, M.; Kohno, Y.; Ando, H.; Urayama, K.; Takigawa, T. *Macromolecules* **2011**, *44*, 8829–8834.
- (12) Ishige, R.; Osada, K.; Tagawa, H.; Niwano, H.; Tokita, M.; Watanabe, J. *Macromolecules* **2008**, *41*, 7566–7570.
- (13) Ren, W.; McMullan, P. J.; Griffin, A. C. *Macromol. Chem. Phys.* **2008**, *209*, 1896–1899.
- (14) Hiraoka, K.; Kobayasi, M.; Kazama, R.; Finkelmann, H. *Macromolecules* **2009**, *42*, 5600–5604.
- (15) Terentjev, E. M.; Wamer, M. *Eur. Phys. J. B* **1999**, *8*, 595–601.
- (16) Kelly, S. M. *J. Mater. Chem.* **1995**, *5*, 2047–2073.
- (17) Yang, H.; Buguin, A.; Taulemesse, J.-M.; Kaneko, K.; Mery, S.; Bergeret, A.; Keller, P. *J. Am. Chem. Soc.* **2009**, *131*, 15000–15004.
- (18) Ohm, C.; Serra, C.; Zentel, R. *Adv. Mater.* **2009**, *21*, 4859–4862.
- (19) Sanchez-Ferrer, A.; Fischl, T.; Stubenrauch, M.; Wurmus, H.; Hoffmann, M.; Finkelmann, H. *Macromol. Chem. Phys.* **2009**, *210*, 1671–1677.
- (20) Bufuin, A.; Li, M.-H.; Silberzan, P.; Ladoux, B.; Keller, P. *J. Am. Chem. Soc.* **2006**, *128*, 1088–1089.
- (21) Ohm, C.; Kapernaum, N.; Nonnenmacher, D.; Giesselmann, F.; Serra, C.; Zentel, R. *J. Am. Chem. Soc.* **2011**, *133*, 5305–5311.

- (22) Ahn, S.; Deshmukh, P.; Gopinadhan, M.; O.Suji, C.; M.Kasi, R. *NANO* **2011**, *5*, 3085–3095.
- (23) Burke, K. A.; Mather, P. T. *J. Mater. Chem.* **2010**, *20*, 3449–3457.
- (24) Chambers, M.; Verduzco, R.; Gleeson, J. T.; Sprunt, S.; Jakli, A. *Adv. Mater.* **2009**, *21*, 1622–1626.
- (25) Hiraoka, K.; Sagano, W.; Nose, T.; Finkelmann, H. *Macromolecules* **2005**, *38*, 7352–7357.
- (26) Schmidtke, J.; Kniesel, S.; Finkelmann, H. *Macromolecules* **2005**, *38*, 1357–1363.
- (27) Cicuta, P.; Tajbakhsh, A. R.; Terentjev, E. M. *Phys. Rev. E* **2002**, *65*, 051704.
- (28) Bermel, P. A.; Warner, M. *Phys. Rev. E* **2002**, *65*, 056614.
- (29) Ohm, C.; Brehmer, M.; Zentel, R. *Adv. Mater.* **2010**, *22*, 3366–3387.
- (30) Mirfakhrai, T.; Madden, J. D. M.; Baughman, R. H. *Mater. Today* **2007**, *10*, 30–38.
- (31) Agez, G.; Mitov, M. *J. Phys. Chem. B* **2011**, *115*, 6421–6426.
- (32) Fan, B.; Vartak, S.; Eakin, J. N.; Faris, S. M. *Appl. Phys. Lett.* **2008**, *92*, 061101.
- (33) Xiao, J. M.; Zhao, D. Y.; Cao, H.; Yang, H. *Liq. Cryst.* **2007**, *34*, 473–477.
- (34) Zografopoulos, D. C.; Kriezies, E. E.; Mitov, M.; Binet, C. *Phys. Rev. E* **2006**, *73*, 061701.
- (35) John, W. D. S.; Fritz, W. J.; Lu, Z. J.; Yang, D. K. *Phys. Rev. E* **1995**, *51*, 1191.
- (36) Broer, D. J.; Lub, J.; Mol, G. N. *Nature* **1995**, *378*, 467–469.
- (37) Hu, W.; Zhao, H. Y.; Song, L.; Yang, Z.; Cao, H.; Cheng, Z. H.; Liu, Q.; Yang, H. *Adv. Mater.* **2010**, *22*, 468–472.
- (38) Bian, Z. Y.; Li, K. X.; Huang, W.; Cao, H.; Yang, H. *Appl. Phys. Lett.* **2007**, *91*, 201908.
- (39) Guo, R. W.; Li, K. X.; Cao, H.; Wu, X. J.; Wang, G. J.; Cheng, Z. H.; Wang, F. F.; Zhang, H. Q.; Yang, H. *Polymer* **2010**, *51*, 5990–5996.
- (40) Akagi, K. *Chem. Rev.* **2009**, *109*, 5354–5401.
- (41) Barnett, D. S.; Schaus, S. E. *Org. Lett.* **2011**, *13*, 4020–4023.
- (42) Han, Y.; Pacheco, K.; Bastiaansen, C. W. M.; Broer, D. J.; Sijbesma, R. P. *J. Am. Chem. Soc.* **2010**, *132*, 2961–2967.
- (43) Guo, R. W.; Cao, H.; Liu, H. J.; Li, K. X.; Huang, W.; Xiao, J. M.; Yuan, X. T.; Yang, Z.; Yang, H. *Liq. Cryst.* **2009**, *36*, 939–946.
- (44) Broer, D. J.; Boven, J.; Mol, G. N. *Makromol. Chem.* **1989**, *190*, 2255–2268.
- (45) Mao, Y.; Warner, M. *Phys. Rev. Lett.* **2000**, *84*, 5335–5338.
- (46) Kahn, F. J. *Appl. Phys. Lett.* **1973**, *22*, 386–388.
- (47) Warner, M.; Terentjev, E. M.; Meyer, R. B.; Mao, Y. *Phys. Rev. Lett.* **2000**, *85*, 2320–2323.
- (48) Kumar, G.; Neckers, D. *Chem. Rev.* **1989**, *89*, 1915–1937.
- (49) Cano, R.; Soc, B.; Minearal, F. *Crystallography* **1968**, *91*, 20–27.
- (50) Xu, J.; Toh, C. L.; Liu, X.; Wang, S.; He, C.; Lu, X. *Macromolecules* **2005**, *38*, 1684–1690.
- (51) Vashchenko, V.; Drushlyak, T.; Shkolnikova, N.; Kutulya, L. *Mol. Cryst. Liq. Cryst.* **1999**, *328*, 245–253.
- (52) Januszko, A.; Kaszynski, P.; Drzewinski, W. *J. Mater. Chem.* **2006**, *16*, 452–461.